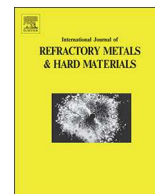




Contents lists available at ScienceDirect

International Journal of Refractory Metals & Hard Materials

journal homepage: www.elsevier.com/locate/IJRMHM

The brittle-to-ductile transition in cold-rolled tungsten sheets: On the loss of room-temperature ductility after annealing and the phenomenon of 45° embrittlement

Carsten Bonnekoh^{a,*}, Philipp Lied^a, Wolfgang Pantleon^b, Thomas Karcher^a, Harald Leiste^a, Andreas Hoffmann^c, Jens Reiser^a, Michael Rieth^a

^a Institute for Applied Materials – Applied Materials Physics, Karlsruhe Institute of Technology, 76344 Eggenstein-Leopoldshafen, Germany

^b Section of Materials and Surface Engineering, Department of Mechanical Engineering, Technical University of Denmark, 2800 Kongens Lyngby, Denmark

^c Plansee, SE 6600 Reutte, Austria

ARTICLE INFO

Keywords:

Isothermal heat treatment
Recovery
Softening kinetics
Apparent activation volume
Annealing texture

ABSTRACT

The high brittle-to-ductile transition (BDT) temperature of conventionally produced tungsten (W), challenges the design of W-based structural components. Recent studies have demonstrated the potential of cold rolling to produce W sheets, which are ductile at room temperature and exhibit a BDT temperature of 208 K. In order to assess the thermal stability of these materials, we conducted isothermal heat treatments (at 1300 K, for annealing durations between 0.1 h and 210 h) combined with studies on the evolution of mechanical properties and microstructure of a severely deformed undoped W sheet. With this work, we demonstrate the need for a stabilized microstructure before utilization of cold-rolled W in high-temperature applications can take place successfully. After annealing at 1300 K for 6 h, the material properties changed remarkably: The BDT temperature increases from 208 K to 473 K and the sharp BDT of the as-rolled condition transforms into a wide transition regime spanning over more than 200 K. This means in fact, an endangered structural integrity at room temperature. We also address the so-called phenomenon of 45° embrittlement of W sheets. Here we show that cleavage fracture in strongly textured W sheets always takes place with an inclination angle of 45° to the rolling direction, independent of the studied material condition, whether as-rolled or annealed. An in-depth study of the microstructure indicates a correlation between an increased BDT temperature caused by annealing and microstructural coarsening presumably by extended recovery. We conclude that 45° embrittlement needs to be comprehended as a combined effect of an increased spacing between grain boundaries along the crack front, leading to an increased BDT, and a high orientation density of the rotated cube component or texture components close to that, which determine the preferred crack propagation of 45° to the rolling direction.

1. Introduction

The brittle-to-ductile transition (BDT) is a striking feature of body-centered cubic (bcc) metals [1]. Because of its impact on the safe operation of components, the BDT is the most critical property of bcc metals from an industrial point of view. Above the BDT temperature, bcc metals behave similarly to face-centered cubic metals: they exhibit a high toughness and good formability [2]. However, below the BDT temperature, the mechanical properties of bcc metals change fundamentally: they exhibit brittle material behavior with unstable crack propagation by cleavage fracture. This change in material behavior

disqualifies bcc metals from being used as structural materials for applications below the respective BDT temperature [3]. The BDT temperature is not an intrinsic property, it is instead strongly influenced by the microstructure and, due to that, by the processing history [4]. On the production side, chemical composition, plastic strain conducted by the forming process and forming temperature are the most critical parameters to control the BDT temperature of the later product [5,6]. Significant improvements in terms of a reduced BDT temperature have been obtained for technical pure W by cold rolling [7–12]. Microstructural investigations have shown that a small grain boundary spacing along the crack front and high dislocation densities are desirable

* Corresponding author at: Institute for Applied Materials – Applied Materials Physics, Karlsruhe Institute of Technology, Hermann-von-Helmholtz-Platz 1, 76344 Eggenstein-Leopoldshafen, Germany.

E-mail addresses: carsten.bonnekoh@kit.edu (C. Bonnekoh), philipp.lied@kit.edu (P. Lied), pawo@dtu.dk (W. Pantleon), t.karcher@tsf.de (T. Karcher), harald.leiste@kit.edu (H. Leiste), andreas.hoffmann@plansee.com (A. Hoffmann), jens.reiser@kit.edu (J. Reiser), michael.rieth@kit.edu (M. Rieth).

<https://doi.org/10.1016/j.ijrmhm.2020.105347>

Received 20 March 2020; Received in revised form 3 August 2020; Accepted 7 August 2020

Available online 15 August 2020

0263-4368/© 2020 The Author(s). Published by Elsevier Ltd. This is an open access article under the CC BY license (<http://creativecommons.org/licenses/by/4.0/>).

microstructural features to achieve room-temperature ductility [13].

On the other hand, induction of high grain boundary and dislocation densities by cold rolling, increase the internal stored energy and consequently the driving force for recrystallization [14]. Moreover, deformation induced HABs are generally higher energetically than grain boundaries formed during primary recrystallization [14]. This might raise problems with the thermal stability of the microstructure of cold-rolled W, aiming to be used in high-temperature environments [15–17]. The replacement of the deformed microstructure by non-deformed grains during recrystallization causes a loss of the improvements gained by the prior deformation [7,18–20]. Alfonso et al. [21,22] have demonstrated the negative impact of an increased level of thickness reduction on the resistance to recrystallization by studies on warm-rolled, technically pure W plates with moderate and high thickness reductions of 67% and 90%, respectively. Considering half recrystallization after an extrapolated operation time of 2 years, i.e. recrystallization of less than 50% of volume fraction during this period as a limit, Alfonso et al. determined a maximum temperature of 1348 K for W that has undergone a thickness reduction of 67%, whereas a limiting temperature of only 1173 K was predicted for the plate with a 90% thickness reduction.

In previous work, we have demonstrated the enormous potential of cold rolling by decreasing the BDT temperature of technically pure W to 208 K [10], which means, in fact, stable crack propagation at room temperature. A cumulative thickness reduction of 98% by severe warm- and cold rolling was carried out to gain this level of improvement. Consequently, the opposing consequences of severe rolling have to be taken into account: Grain size reduction and the increase in dislocation density achieve the desired ductile W at room temperature [13] on the one hand. The negative impact of such microstructures on the thermal stability, on the other hand, raises questions about the mechanical performance of severely cold-rolled W sheets at room-temperature after exposure to heat. In addition, rolled W sheets are frequently facing a specific problem of fracture after subsequent heat treatment: This phenomenon has become known as 45° embrittlement, due to the characteristic crack path of cleavage fractures with an inclination angle of 45° with respect to the rolling direction [23]. With this paper, we attempt to answer the following open questions:

- (1) What is the effect of heat treatments over short to intermediate periods of time on the BDT temperature and the microstructure of cold-rolled, room-temperature ductile W sheets?
- (2) What is the origin of 45° embrittlement?

This paper is organized as follows: After a first assessment of the softening behavior of cold-rolled W sheets during subsequent annealing, we study the impact of annealing and related softening on the BDT temperature. Then, we show the results of a comprehensive microstructural characterization and make an attempt to link the evolution of the microstructure with the change in BDT temperature and the occurrence of 45° embrittlement.

2. Materials and methods

In this study, we used an initially warm-rolled and subsequently cold-rolled, technically pure W sheet as starting material. For the distinction between warm- and cold rolling, we make use of the classification for bcc refractory metals by Trefilov et al. [24]. The material was provided by Plansee SE, Reutte, Austria. The total logarithmic strain conducted by warm- and cold rolling was 4.1, of which the initial 3.3 were obtained by warm rolling and the last 0.8 by cold rolling. This is equivalent to a total thickness reduction of 98% after the last pass of cold rolling. The thickness of the sheet after rolling was 0.1 mm. We refer the reader to another publication for more details of the processing history [10]. The hardness of the cold-rolled material in the as-rolled condition was 646 ± 7 HV0.1. The chemical composition after rolling is given in Table 1.

Table 1

Chemical analysis of the as-rolled condition taken from Ref. [25].

C	N	O	Al	Si	P	S	K	Ca	V
7	< 2	7	< 2	< 10	< 3	< 2	< 1	1.5	< 0.05
Cr	Mn	Fe	Ni	Cu	Zn	Mo	Cd	Pb	
1.0	0.3	12	0.8	0.07	< 0.5	22.1	< 0.03	< 0.03	

All concentrations are given in wt.-ppm. Summing up the concentrations of impurities considers the measured concentration or the detection limits (<) depending on which one is higher. Foreign elements in total: 72.4 wt.-ppm

2.1. Material: heat treatments

Heat treatments at 1300 K, which is equivalent to 35% of the melting temperature, were carried out. Annealing durations in the range from 0.1 h to 210 h were undertaken. Two different procedures were applied: (i) for annealing durations up to 50 h, we used a tube furnace. The furnace was heated up to the target temperature of 1300 K. After the furnace thermocouples indicated reaching the target temperature, the specimens placed in an evacuated tube were inserted into the furnace. Time measurement started after the difference between the actual temperature of the specimen (measured by a thermocouple in the slider located below the crucible) and the target temperature was less than 20 K. (ii) Heat treatments with annealing durations longer than 50 h were conducted in a muffle furnace, after encapsulating the specimens in glass ampoules. The encapsulation included flushing the ampoules with argon, then evacuation and sealing with a blowtorch. In both procedures, the tube and the ampoules were cooled down in air after extraction from the furnace.

2.2. Vickers hardness tests: softening behavior

In preparation for Vickers hardness tests, the differently heat-treated specimens were embedded in a hard compound as a mechanically clamped stack of specimens. The material volume of the specimens affected by electro-discharge machining was removed by careful grinding of the stack of samples. Due to mechanical and subsequent electrochemical polishing, we ensure smooth sample surfaces (surface roughness R_t below 100 nm) and minimal hardening of the surface layer by preparation-induced deformation. An aqueous solution containing demineralized H₂O and 0.66 wt.-% NaOH (diluted ASTM electrolyte VII-7 [26]) was used as etching agent. We applied a voltage of 10 V for a net time of 180 s, activated in intervals of 5 s current and 10 s time-out. The Vickers hardness (HV0.1) of the samples was determined at room temperature using a combined Vickers microhardness indentation and measuring system (Clemex CMT.HD, Canada) providing a 400× optical magnification. A load of 100 gf for a standard dwell time of 10 s was applied [27]. In order to maximize the number of interacting grains, indentation was performed along the rolling direction (RD) on the surface defined by the transversal direction (TD) and normal direction (ND). The indents were conducted on the centerline parallel to the transversal direction of the above-noted TD-ND cross-section. For each condition, the mean value out of 10 data points was calculated after the elimination of maximum and minimum value out of a set of 12 indentations.

2.3. Fracture mechanical testing: BDT temperature

Detailed descriptions of the single-edge notched tensile SE(T) specimens and the specimen fixture are provided in Fig. 1. First, the sample geometry of the SE(T) specimens was cut out. Afterwards, the cut parts were annealed at 1300 K for 6 h in a tube furnace. Finally, the starting notch was inserted by EDM. The tip of the notch had a radius of around 70 μm and showed multiple parallel-aligned thermal-induced cracks as highlighted in Fig. 1c. Only the L-T crack system [28] was studied in this work. To determine the impact of the annealing on the BDT

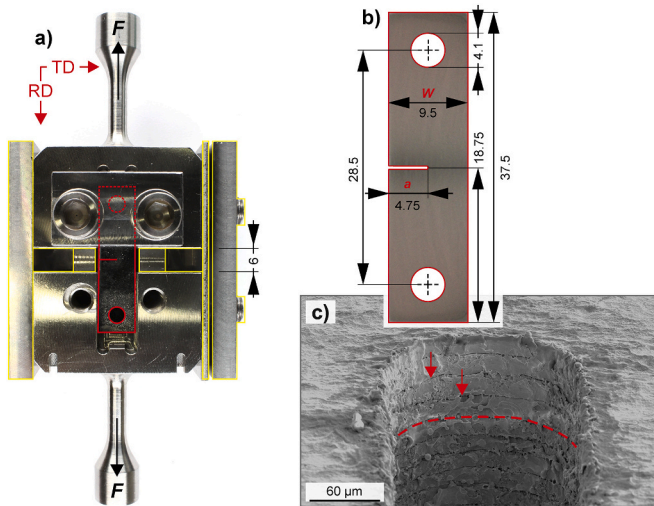


Fig. 1. Fracture mechanical testing. In (a) the specimen fixture, specimen position, and the assembly device are depicted. The SE(T) specimen is highlighted in red, components of the assembly device are bordered by yellow lines. Furthermore, the alignment of the rolling direction (RD) and transverse direction (TD) with respect to the notch position is provided. In (b) the geometry of the used SE(T) specimens is described in detail. Subplot (c) shows the tip of the notch inserted by EDM. (For interpretation of the references to colour in this figure legend, the reader is referred to the web version of this article.)

temperature, we conducted a series of fracture toughness tests (mode I loading, crack opening). The tests were performed in air at a nominal loading rate of $1 \text{ MPa m}^{0.5} \text{ s}^{-1}$ until fracture occurred. We conducted all fracture toughness test in displacement-controlled mode with constant crosshead speed. A universal mechanical testing machine (ZwickRoell 1474, Germany) equipped with an environmental chamber (Instron SFL 3119-400, USA) was used for all fracture toughness tests, covering a temperature range 120–550 K. Values for the critical stress intensity factor (K_{IC}) were calculated in accordance with ASTM E399 [28]. Literature does not provide a consistent criterion for the transition temperature. In this study, we define the BDT temperature as the lowest test temperature in the respective test campaign that showed only specimens exhibiting ductile or stable crack propagation across at least 2% of the ligament width [29], in this work denoted as semi-ductile material behavior. Or in other words: The lowest test temperature at which samples did not exhibit brittle fracture. For the distinction in ductile, semi-ductile, and brittle material samples we made, we refer the reader to an earlier publication [10].

2.4. Electron backscatter diffraction: texture and microstructure

Sample preparation for the EBSD experiments was conducted in the same way as above described for the Vickers hardness measurements. Data on the materials' microstructure and texture were collected with a high-resolution field emission SEM MERLIN (Carl Zeiss Microscopy, Germany) equipped with a high-speed data collection EBSD system Hikari XP (EDAX Inc., USA). Acquisition of orientation information for texture determination was carried out on the cross-section defined by TD and ND [28], using an acceleration voltage of 20 kV and probe current of 20 nA. With regard to the grain dimensions, step size for texture measurement was set to 400 nm [30]. Ten maps, with an area of $280 \mu\text{m}$ by $40 \mu\text{m}$ each, were acquired along the centerline of each sheet, collecting orientation data of about 10k grains [31]. Microstructure analysis was performed using an acceleration voltage of 15 kV, probe current of 20 nA and a step size of 40 nm. Cross-sections defined by RD and ND [28] were scanned. Four maps, with an area of $35 \mu\text{m}$ by $45 \mu\text{m}$ each, were acquired along the centerline of the sheet. Texture and mean grain size were derived from stitched maps [32].

Error bars were determined by calculating the standard deviation between the mean values of the single maps. By using TSL OIM Analysis v8, pixels with a confidence index (CI) below 0.1 were eliminated during post-processing. Apart from a grain CI standardization, no clean-up routine was performed on the datasets so that the measured orientation of all the points remained unchanged. Before texture analysis, orientation data was adjusted for slight specimen misalignment in the SEM inspecting the symmetry of the discrete pole figures [33]. Orientation distribution functions (ODF) were calculated using the generalized spherical harmonic series expansion of Bunge [34] expanded up to rank 34 and selecting a Gaussian half-width of 5° for smoothing, which is the lowest value without obvious artifacts in the maps displaying the ODF at rank 34 for these materials [35]. In this paper, high-angle boundaries (HABs) are defined as boundaries between points with a lattice disorientation angle above 15° , low-angle boundaries (LABs) are defined to have lattice disorientation angles between 2° and 15° . We selected the line intercept method to determine the mean spacing between intersection points along test lines along ND with HABs and LABs. The expression chord length frequently used in this paper refers to the spacing between boundaries along ND, determined along multiple intersecting lines. Here, we differentiate between (i) the interception distance between HABs, denoted as chord length for HABs and (ii) the spacing considering both, HABs and LABs, called chord length for all boundaries. Due to the alignment of the L-T crack system used in this study, the mean chord length for HABs represents the mean spacing between HABs (i.e. lattice disorientations above 15° , cf. Ref. [14]) along the crack front. Similar to that, the mean chord length for all boundaries represents the mean spacing between boundaries with lattice disorientation angles above 2° along the crack front.

2.5. X-ray diffraction experiments: dislocation density

The dislocation density was assessed by X-ray diffraction (XRD) and derived from the peak broadening of the resulting line profile. Due to the smooth surface of the rolling plane after cold rolling and pickling, electrochemical polishing as described above was sufficient as surface preparation. A Bragg-Brentano type diffractometer (Seifert, Germany) equipped with a 1D detector (Meteor 1D; 600 single active segments of 0.01°) was used for recording the line profiles. The diffractometer was equipped with a Cu anode, operating with an acceleration voltage of 40 kV to gain an optimized ratio of intensities between CuK_α and bremsstrahlung. The beam current was 30 mA. A Ni filter was used to suppress CuK_β radiation during the experiment, whereas the $\text{CuK}_{\alpha 2}$ fraction was subtracted during post-processing applying the mathematical Rachinger correction using Seifert Rayflex Analyze in version 2.503, cf. Ref. [36]. The specimen was mounted on the Goniometer (Type MZ IV) so that the rolling plane (plane normal to ND) was facing the X-ray beam. Due to the symmetrical beam path, the diffraction vector is parallel ND. A 2θ interval between 10° and 135° was scanned with a step size of 0.01° . Due to the use of a 1D detector, an interval of 6° (2θ) was measured at once. The cumulated acquisition time for each angular step was 360 s. We corrected the entire full width half maximum (FWHM) of each peak by subtracting the instrumental contribution applying the approach for Lorentz-shaped peaks (linear subtraction), i.e. the physical width is underestimated and due to that the dislocation density as well [37]. Instrumental line broadening was quantified measuring the powder standard NIST SRM 660c (LaB_6 , line position, and line shape standard). After this correction, we calculated the dislocation density by applying the modified Williamson-Hall method [38]. Due to texture sharpening during annealing, fewer peaks were accessible in the present study compared to the previous work dealing with the as-rolled state [13]. The three most dominant peaks relating to the $\{200\}$, $\{211\}$, and $\{222\}$ plane, were considered for the calculation. The dimensionless screening factor M , characterizing the effective outer cut-off radius, was assumed to be 2 [39].

3. Results and discussion

In this study, we elucidate the impact of short- to intermediate-time annealing durations in the range of 0.1–210 h on cold-rolled tungsten (W) sheets. The following results concern (i) mechanical properties with hardness and brittle-to-ductile-transition (BDT) temperature, and (ii) microstructural properties like texture and chord length, before and after an isothermal heat treatment at 1300 K. In addition, differences in the crack path are studied based on a post-mortem study of SE(T) specimens and whole W sheets. The evolution in microstructure and material behavior during annealing are discussed on the background of the phenomenon of 45° embrittlement.

3.1. Softening kinetics

In this section, we discuss the hardness loss of a cold-rolled W sheet during isothermal heat treatments conducted at 1300 K. Vickers hardness tests were carried out to get indirect information about the microstructural changes during annealing. Our results show a remarkable loss of hardness compared to the as-rolled state even at the onset of annealing.

Fig. 1a displays the effect of isothermal heat treatments at 1300 K on the Vickers hardness ($HV_{0.1}$) of cold-rolled W for heat treatments between 0.1 h and 210 h. In the as-rolled condition, the studied material possesses an initial hardness of 646 ± 7 HV0.1. In comparison to conventionally warm-rolled W plates possessing values from (430 HV10) [21,22] to (550 HV0.5) [40], a hardness of 646 HV0.1 represents a significant hardening, which almost reaches values of drawn W wires (680 HV0.5) [41]. This initial hardness of the as-rolled condition of 646 ± 7 HV0.1 matches with previous studies of cold-rolled W sheets [17,40,42,43] and seems characteristic for them. These high hardness values are a consequence of the ultrafine-grained and dislocation-rich microstructure of such W sheets, which forms during cold rolling [13]. However, for this comparison the differently used loads and due to that the difference in indentation size must be considered, which however usually gains noticeably influence only for hardness testing with low loads below 100 gf [44]. The high hardness is a unique feature of the as-rolled state and is rapidly lost after a short annealing at 1300 K. After an annealing duration of only 0.1 h, the hardness dropped by 100 HV0.1 to values around 560 HV0.1. However, after this first loss of hardness, the rate of softening slows down for longer annealing durations. For heat treatments beyond 50 h, the determined values do not follow the logarithmic decrease of the beginning. We interpret this deviation as an undesired effect caused by the change in experimental method: For heat treatments longer than 50 h, we switched from annealing in the tube furnace to annealing in the muffle furnace.

In the first stage of thermally activated softening of polycrystalline materials, the loss in hardness often progresses in a logarithmic manner, (Eq. (1)). This $\ln(t)$ dependence, has been elucidated by Kuhlmann for the softening by thermally activated dislocation-based processes [45,46]. Aside from the logarithmic dependence of the hardness HV_{rec} on time t , Eq. (1) also includes parameters HV_0^* and c_1 , where HV_0^* is a back-extrapolated hardness value and c_1 a measure of the ongoing recovery kinetics.

$$HV_{\text{rec}} = HV_0^* - c_1 \ln(t) \quad (1)$$

The trend line plotted in Fig. 2 shows the regression line of the experimental data. The match of data and trend line reveals that a logarithmic relationship is suited to describe the softening behavior of cold-rolled W sheets for annealing durations between 0.1 and 50 h. Annealing for 100 h and 210 h were excluded in this attempt due to the change of furnace for longer annealing durations. The parameter c_1 is temperature-dependent and increases with increased annealing temperature [47]. Normalizing c_1 by the annealing temperature results in a nearly temperature-independent material property c_1/T , which reflects

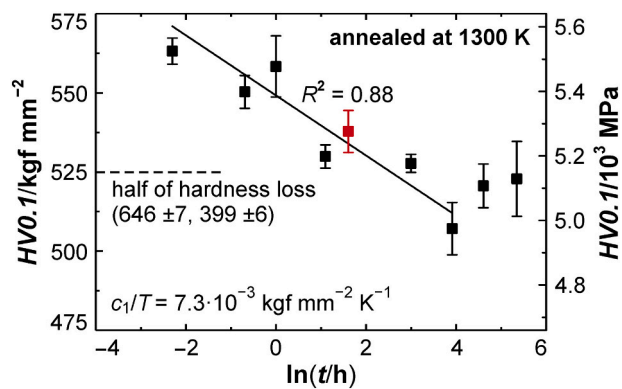


Fig. 2. Hardness evolution during isothermal annealing. The Vickers hardness ($HV_{0.1}$) for cold-rolled W specimens with subsequent heat treatment is plotted against the annealing time (t) at a constant annealing temperature at 1300 K. The trend line of the recovery behavior was calculated based on the logarithmic time dependence of Kuhlmann. The red symbol (annealing duration of 6 h) highlights the material condition, which was selected to assess the impact of heat treatment on the BDT temperature and the microstructure of cold-rolled W sheets. The error bars display the standard deviation of the mean values, which were calculated out of 10 single Vickers hardness measurements per annealed specimen. (For interpretation of the references to colour in this figure legend, the reader is referred to the web version of this article.)

the microstructure-dependent softening kinetics of the studied material [21]. Furthermore, an apparent activation volume denoted as V_a , can be calculated in accordance with the relationship shown in Eq. (2), where k_B is the Boltzmann constant and the approximated prefactor 3 is given due to the use of Vickers hardness instead of yield pressure [14,48]. Please note the slightly declining trend of the prefactor with decreasing load applied during the hardness test [49].

$$V_a = 3 \frac{k_B}{c_1/T} \quad (2)$$

The deduced apparent activation volume allows a comparison of softening kinetics obtained in different studies. From the regression line shown in Fig. 2 for a thickness reduction of 98%, an apparent activation volume of $28b^3$, 0.58 nm^3 was derived (where b is the length of the Burgers vector, which is 0.274 nm for $\frac{1}{2}\langle 111 \rangle$ dislocations in W), which is equivalent to a value of $28b^2$ and 2.1 nm^2 for the apparent activation area (V_a/b). The apparent activation volume of $28b^3$ matches well the $32 \pm 7b^3$ derived from the c_1/T values (at 873 K, 1073 K, and 1423 K) provided by Reiser et al. [50] for the same batch of material. Our result is consistent with the trend of warm-rolled W by Alfonso et al. [21,22,51]. Their studies have revealed a decrease in apparent activation volume with increasing rolling deformation as expected due to an increase of the dislocation density. For sheets with a thickness reduction of 67% and 90% conducted by warm rolling, apparent activation volumes of $66b^3$, 1.4 nm^3 and $48b^3$, 1.0 nm^3 , respectively, have been reported. Consequently, we can point out the tendency of W to possess lower apparent activation volumes with increasing strain conducted by rolling. Referring this tendency to the apparent activation area, a reduction of the mean area swept by the dislocation on its way before annihilation is indicated [52]. The decreasing apparent activation volume implies an acceleration of the softening behavior with increasing level of pre-deformation conducted by warm rolling or a combination of warm- and cold rolling, respectively.

In comparison with previous studies on warm-rolled W sheets, the loss of hardness at the onset of softening is several times higher in the present study (-140 HV0.1). Alfonso et al. have reported only slightly reduced hardness values, of around -30 HV10, during recovery [21,22]. However, after the initial drop, which took place until an annealing duration of 0.1 h and has not been observed for warm-rolled W sheets [21,22], the loss of hardness in our sheets (-40 HV0.1) is

comparable to the loss of hardness in the early stage of the quoted references (-30 HV10). It seems that similar to the high hardness of the as-rolled state, the observed rapid loss of hardness is a feature of severely deformed W sheets. Ciucani et al. [40] reported comparable values for the loss of hardness (-163 HV0.5) at the beginning of softening for a cold-rolled W sheet (0.2 mm thick) with an initial hardness of 642 HV0.5. Additionally, the approximately constant level of the standard deviation of the mean hardness values during annealing between 0.1 h and 50 h points to a homogeneously occurring process responsible for the observed material softening. This is different to materials, which undergo e.g. discontinuous recrystallization, possessing recrystallized (soft) and recovered (hard) regions at the same time, causing an increased level of the standard deviation as long as both conditions coexist.

In the studied timeframe of annealing (up to 210 h) no further drop in hardness, indicating the onset of following processes like discontinuous recrystallization or grain growth was observed (cf. Ref. [53]). Furthermore, even after the maximum annealing duration of 210 h, the material has an increased hardness (550 HV0.1) compared to fully recrystallized W (400 HV0.1). Possible explanations for this phenomenon might be the strong loss in hardness at the onset of softening and an accompanying reduction of internal stored energy to a large extent. This reduces the driving force for discontinuous recrystallization and might delay its onset [54].

Although the loss in hardness of cold-rolled W exceeds the values, which have been reported for warm-rolled W [21,22], the softening kinetic gives strong indications that loss in hardness of cold-rolled W follows a mechanism that is closely linked with recovery. This conclusion is derived based on the observations that (i) the loss in hardness possesses a logarithmic time dependence and (ii) the microstructural process responsible for the softening takes place homogeneously, leading to only slight scattering of the single hardness values determined for the same specimen (low standard deviation). Both are well-known characteristics of recovery [53].

3.2. BDT and regime-related inclination of the crack path

In this section, we study BDT temperature and crack paths of cold-rolled W in as-rolled condition and after annealing at 1300 K for 6 h. Our fracture toughness tests show a change in BDT caused by the heat treatment: the sharp transition from brittle to ductile material behavior as observed for the as-rolled material condition transforms into a wide transition regime. The BDT temperature, representing the lowest test temperature exhibiting not any brittle material behavior during our experiments, is shifted from 208 K for the as-rolled condition to 473 K after annealing. After annealing, specimens tested at room temperature show brittle material behavior and characteristic crack propagation along 45° to the rolling direction.

Figure 3 displays trends of the critical stress intensity factor (K_Q) versus test temperature (T) for the as-rolled and annealed material. All results in this section representing the annealed state are acquired from samples that were heat-treated at 1300 K for 6 h (cf. Fig. 2). The results of the as-rolled condition have been published in earlier work [10] and are shown as a reference. Cold-rolled W in as-rolled condition possesses a sharp BDT, i. e. narrow transition regime spreading over about 25 K only. The BDT temperature before annealing is 208 K. After annealing, however, the material does not exhibit a sharp transition between the brittle and the ductile regime anymore. Based on the data shown in Fig. 3, three temperature regimes can be identified for the annealed material: (i) in the low-temperature regime with an upper bound temperature of 235 K, all specimens exhibited brittle material behavior (filled symbols); (iii) starting at 460 K and for test temperatures above solely ductile material behavior (open symbols) was observed. Consequently, regime (ii) spans over a wide temperature range in between the abovementioned temperatures. This transition regime covers a temperature range of more than 200 K which contains specimens

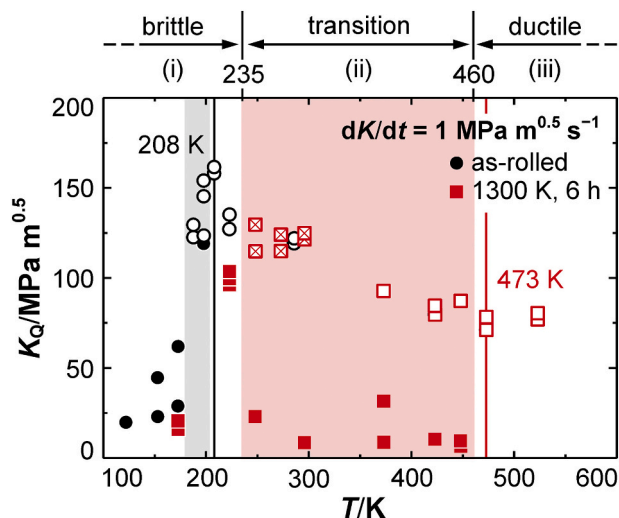


Fig. 3. BDT of cold-rolled W before and after annealing. The critical stress intensity factor (K_Q) is plotted against the test temperature (T) applied for performing the single fracture toughness tests. Two material conditions are displayed: samples in the as-rolled condition (black circles) and samples heat-treated for 6 h at 1300 K (red squares). Filled symbols indicate brittle material behavior, crossed symbols and open symbols signalize semi-ductile and ductile material behavior, respectively. The regime marked by grey or red shading is referred to as the transition regime. All fracture toughness tests were carried out at a constant loading rate (dK/dt). The as-rolled experiments have been published earlier in Ref. [10], where also the distinction between brittle, semi-ductile, and ductile material behaviors is explained. (For interpretation of the references to colour in this figure legend, the reader is referred to the web version of this article.)

fractured in a brittle or ductile manner. Furthermore, unlike the as-rolled condition, also specimens with semi-ductile material behavior (crossed symbols; at least 2% stable crack propagation across the ligament width [29]) were detected after annealing. Consequently, the transition regime from brittle (unstable crack propagation) to ductile material behavior (stable crack growth) is widened by a large extent (compared to the as-rolled W) and the BDT temperature is increased from 208 K to 473 K. As a result, the excellent ductility of the as-rolled condition is lost, which means in effect an endangered structural integrity at room temperature.

In addition, we conducted a post-mortem study of the fracture toughness test specimens to investigate the transition regime (ii) where strongly scattering behavior of the heat treated specimen is observed. Fig. 4 shows the inclinations of the crack path for annealed material (a, b, d, e) and, as a reference, for brittle and ductile specimens of the as-rolled state (c, f). The crack path characteristics for specimens with ductile material behavior (d, e, f) are discussed first. The crack path of annealed materials representing ductile material behavior (d, e) is independent of the test temperature regime. Different crack patterns are not recognized between the ductile specimen tested in the transition regime (ii) displayed in (d) and for specimens that were tested above 460 K (e). In both cases, the crack propagates approximately normal to the applied tension through the ligament width [28]. The ductile specimens of the as-rolled state (f) exhibit an almost perfect crack growth in the extension of the crack-starting notch as well. Thus, we conclude for rolled W sheets tested in this manner that stable crack growth is characterized by crack propagation normal to the applied tension.

Next, we discuss the crack paths of specimens tested in regime (i), i.e. below 235 K, in the case of the annealed material (a) and below 180 K for the as-rolled material (c). In this mentioned regime the materials showed solely brittle material behavior. Again, crack paths of the annealed (a) and the as-rolled material (c) show a similar pattern. After crack initiation, the preferred direction of propagation develops an

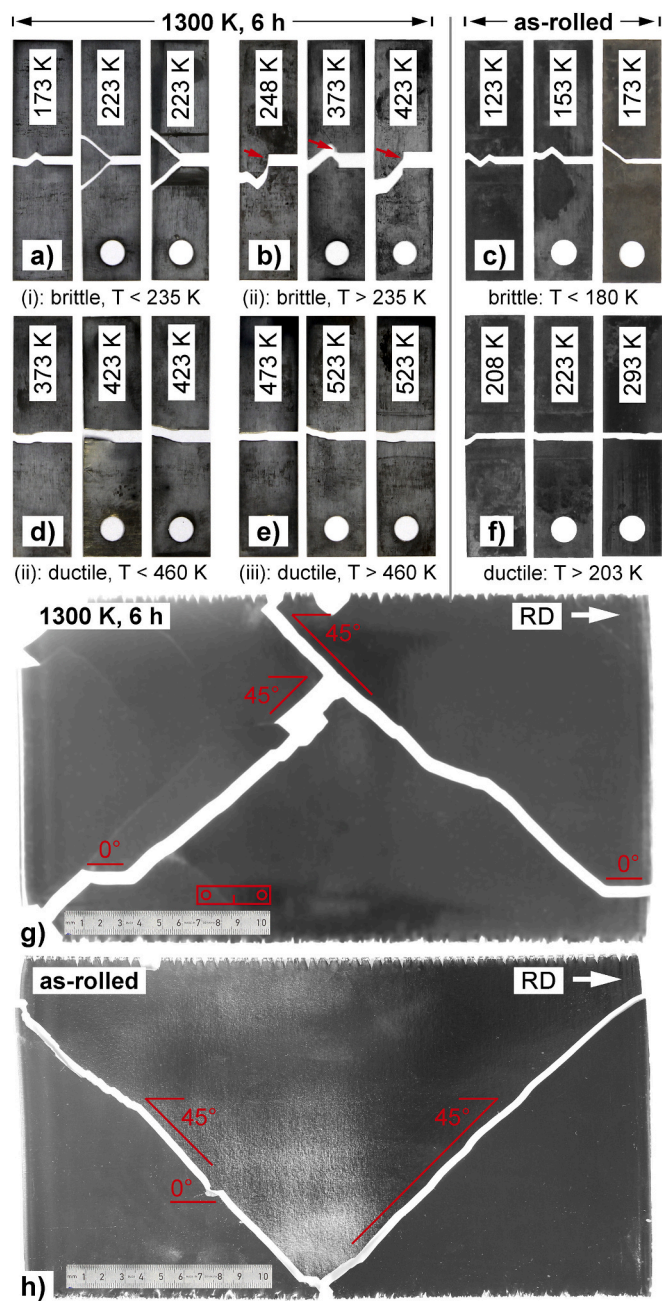


Fig. 4. Crack paths in as-rolled and annealed conditions. A post-mortem investigation of the crack paths of the annealed specimens (a, b, d, e) reveals characteristic alignments of the crack path in the ductile regime (d, e), in the brittle regime (a) and for brittle material behavior above 223 K (b). Examples of ductile (f) and brittle (c) fracture behavior of the as-rolled state are displayed as a reference. The labeling (i)-(iii) refers to the regimes defined in Fig. 2. The propagation paths of cracks in larger sheets are given in (g, h). The sheet annealed at 1300 K for 6 h (g) was subsequently fractured at room temperature. The sheet displayed in (h) maintained in the as-rolled condition and was cooled and loaded in liquid nitrogen to provoke brittle material behavior.

inclination angle of around 45° with respect to the rolling direction in both cases. In tests, which were conducted at test temperatures close to 180 K or 235 K, respectively, the crack propagates in a straight manner from the notch tip towards the outer specimen surface. Studying the fracture surfaces reveals transgranular crack propagation in this regime. Both, 45° fracture and transgranular crack propagation are in accordance with recent observations by Nikolić et al. [11] on ultrafine-grained W sheets (L-T crack system) if tested below the BDT

temperature. With decreasing temperature, the crack paths seem to become zigzag-shaped (Fig. 4a and c, specimens left-hand side); however, they retain the inclination angle of 45° in the single segments. Strikingly, the annealed material exhibit cracks that are split into two individual crack paths (Fig. 4a, specimens at the right-hand side). Both cracks start at the root of the notch and propagate with 45° inclined to the rolling direction, but, in different directions. Apart from this, the annealed and the as-rolled material do not show differences regarding the crack path if fractured in the brittle regime.

Finally, the brittle crack paths of heat-treated specimens tested between 235 K and 460 K (Fig. 4b) are discussed (transition regime). At first glance, there is no clear difference between these specimens and the brittle samples below the maximum K_Q in the annealed (Fig. 4a) and as-rolled (Fig. 4c) conditions. The crack also appears to propagate with an inclination angle of 45°. However, unlike both other brittle states (as-rolled and annealed), brittle crack propagation of regime (ii) seems to occur parallel to the rolling direction at the root of the notch, or the crack kinks (highlighted by red arrows) very close to the notch along the direction of maximum grain elongation, i.e. along the rolling direction. After a macroscopic propagation of the crack, the inclination of the crack path changes to the well-known 45° direction. Propagation along the direction of maximum grain elongation has been already been observed by Gludovatz et al. for fully recrystallized W rods [55]. An EBSD study of the fracture surface (to be published) shows that crack propagation with an inclination of 45° to the rolling direction takes place along {001} cleavage planes and furthermore that the fracture surface parallel to the rolling direction possess a transgranular fracture pattern as well, presumably related to cleavage along {110} planes. Aside from this anomalous crack propagation, no distinguishing feature in the crack path was found which would allow easy discrimination between the as-rolled state and specimens embrittled during annealing.

In order to conclude this section, we discuss the crack paths on the scale of whole sheets. Unlike the SE(T) specimens, we forwent to introduce a notch in preparation for these tests. Fractured sheets are displayed in Fig. 4g and h. Again, the condition annealed at 1300 K for 6 h (Fig. 4g) is benchmarked against an as-rolled material (Fig. 4h). The annealed sheet (Fig. 4g) fractured at room temperature in a typical manner known for severely rolled and heat-treated W sheets that exhibit 45° embrittlement. Most segments of the crack follow an inclination angle of 45° to the rolling direction. As mentioned above, some short zig-zag-shaped crack paths might be caused due to the relatively large temperature difference between the test at room temperature and the BDT temperature at 473 K. The as-rolled sheet (Fig. 4h) with a BDT temperature of 208 K was cooled and loaded in liquid nitrogen (76 K) to provoke brittle material behavior. The results confirm the fracture pattern of the SE(T) specimens described above. Independent of the material condition, whether as-rolled or annealed, brittle material behavior results in a crack growth that propagates with an inclination angle of 45° to the rolling direction. Consequently, we proved that fracture with an inclination angle of 45° to the rolling direction is not triggered by thermal driven processes that weaken the material. Even room-temperature ductile W sheets fracture under 45° to the rolling direction in tests conducted below their BDT temperature, for instance in liquid nitrogen. This result gives a first indication that 45° fracture is not responsible for embrittlement of rolled W sheets after annealing even though the characteristic crack path is first observed after annealing in tests conducted at room temperature. The subject of 45° embrittlement will be conclusively addressed after discussing the texture of the sheets and microstructural changes during heat treatment.

3.3. Texture and microstructure

In order to observe modifications of texture and microstructure of the annealed material used in the campaign of fracture toughness tests, we carried out EBSD and XRD measurements. Here, we focus only on the differences between the as-rolled state and the material annealed at

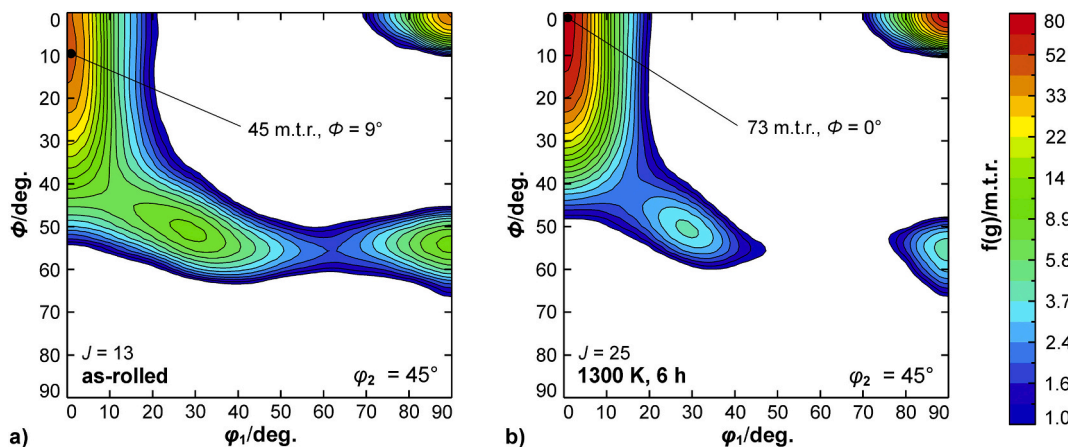


Fig. 5. Evolution of the texture during annealing as characterized by the orientation density function (ODF). Orientation densities are displayed in cross-sections of the Euler space with $\varphi_2 = 45^\circ$. The orientation densities in (a) the as-rolled and (b) the annealed condition after 6 h at 1300 K are shown. The orientation densities are given in multiple times random (m.t.r.). For both materials the texture index (J) is given, describing the sharpness of the texture by a single parameter as described by Bunge [34]. Corresponding pole figures are displayed in Fig. A1 located in the appendix.

1300 K for 6 h. A detailed study of the as-rolled state has been presented earlier [13]. Our results show an increase in the orientation density of texture components of the α -fiber after annealing, particularly the rotated cube component. Furthermore, a collapse of the lamellar microstructure and a reduction of the dislocation density by almost two orders of magnitude was observed after annealing compared to the cold-rolled material.

Fig. 5 shows sections $\varphi_2 = 45^\circ$ of the orientation distribution function (ODF) [34] for (a) the as-rolled and (b) the annealed condition. The distinct fiber texture of the as-rolled state (a) possesses an incomplete, but very strong α -fiber and low orientation density of the components belonging to the γ -fiber. The increase of texture index (J) [34] from 13 to 25 reveals a texture-sharpening during annealing, whereby a texture index of unity signalize a random distribution of crystals orientations and goes towards infinite for a single crystal. Particularly towards the rotated cube component, the orientation density is remarkably increased, reaching a maximum value of 73 m.t.r. (multiple times random). In contrast to that, the γ -fiber loses in orientation density during annealing. As a result of the dominating texture components near the rotated cube component, a large number of grains have a favorable $\{001\}$ cleavage plane [56,57] parallel to the normal direction of the sheet and a cleavage plane inclined 45° or almost 45° to the rolling direction. This is very likely explaining the crack propagation with 45° to the rolling direction for brittle material behavior of strongly textured W sheets as described in the previous section [23]. Fractographic investigations revealing prevalent transgranular fracture support this conclusion.

Furthermore, the evolution of the texture during annealing reveals that the annealing behavior of cold-rolled W sheets differs from the classical picture of recovery describing dislocation-mediated softening processes [53]. Changes in dislocation structure and cell substructure are not expected to cause significant differences in texture [54]. Consequently, the increasing orientation density of the rotated cube component and the weakening of the γ -fiber after 6 h of annealing at 1300 K indicates that beside dislocation annihilation and rearrangement at least one further process is involved during softening of the cold-rolled W sheets observed here.

In order to gain more information about this process, we carried out a detailed microstructural analysis, taking into account chord lengths, boundary densities, and the change in dislocation density. Table 2 summarizes the parameters derived from the EBSD and XRD experiments. As Fig. 6 shows, a remarkable change in the initially lamellar microstructure can be identified after annealing at 1300 K for 6 h. A collapse of the lamellar microstructure took place, leading to

spheroidization of the grains. The aspect ratio RD/ND of the grains decreases remarkably from at least 14 as reported in Ref. [13] for the as-rolled condition to an aspect ratio around 2 or 3. Prangnell et al. [58] have reported for lamellar, HAB-rich deformation structures a break-up of the lamellar microstructure and subdivision of single grains by a LAB-triggered necking process. This break-up of lamellar grains is caused by the surface tension of the less mobile LABs that are aligned transversal to the rolling direction and requires only short-range motion of HABs (cf. Ref. [53]). Park et al. [59] have reported a higher stored energy in γ -fiber grains with respect to grains having an α -fiber orientation. This difference might also influence the collapse of the layered microstructure and the persistence of grains with rotated cube orientation on the cost of grains belonging to the γ -fiber.

In the following, the microstructural evolution is investigated more in detail. The evolution of the mean chord lengths, (i) for all boundaries and (ii) for HABs only and related distributions are treated first. On average, the chord length between all boundaries (including HABs and LABs) is $0.16 \mu\text{m}$ in the as-rolled condition. With a mean chord length for all boundaries of $0.69 \mu\text{m}$, an increase by more than factor 4 was measured after annealing at 1300 K for 6 h indicating a coarsening of the subgrains along this direction. Fig. 7 displays the distributions of the chord lengths for all boundaries for both material conditions: the probability density (P) of the chord length for all boundaries times the mean chord length for all boundaries ($\bar{\lambda}_{\text{all}}$) is plotted versus the chord length for all boundaries (λ_{all}) normalized by the mean chord length for all boundaries. Independent of the material condition, whether as-rolled (Fig. 7a) or annealed (Fig. 7b), the distributions possess a distinct maximum. The displayed data are unimodally distributed and well described by lognormal distributions as shown in Fig. 7. This statement applies to the as-rolled condition and also after the heat treatment. Consequently, restoration processes like discontinuous recrystallization, which are linked to a development of bimodal distributions in partially recrystallized conditions [53], can be excluded from the following discussion about the origin for the collapse of the lamellar microstructure and the starting spheroidization. Instead, the preservation of the unimodally distributed chord length for all boundaries during annealing points to a continuous process.

A similar investigation was applied considering the chord lengths for HABs. The mean chord length for HABs was determined as $0.26 \mu\text{m}$ in the as-rolled condition. For the annealed condition a mean value of $1.9 \mu\text{m}$ was measured. This is an increase by factor 7, which is almost twice the increase of the mean chord length for all boundaries. Analogous to Fig. 7, in Fig. 8a, (for the as-rolled W) and Fig. 8b (representing the annealed condition) the probability density (P) of the

Table 2

Properties of W sheets in the as-rolled and annealed state. Results of the as-rolled sheet are taken from Ref. [13].

Material	T_{BDT}/K	$\bar{\lambda}_{HAB}/\mu m$	$\bar{\lambda}_{all}/\mu m$	$\rho_D/10^{14} m^{-2}$	$S_V/\mu m^{-1}$	$x_{HAB}/-$	$x_{LAB}/-$	$x_{CSL}/-$	$\bar{\theta}/deg.$
As-rolled	208	0.255 ± 0.005	0.159 ± 0.002	8.8	8.12 ± 0.03	0.68 ± 0.02	0.32 ± 0.02	0.079 ± 0.007	29.5 ± 0.6
1300 K, 6 h	473	1.866 ± 0.28	0.694 ± 0.022	0.19	2.29 ± 0.07	0.43 ± 0.02	0.57 ± 0.04	0.052 ± 0.011	19.4 ± 1.3

This table gives a summary of the BDT temperature (T_{BDT}), mean chord lengths ($\bar{\lambda}$) and the dislocation density (ρ_D) before and after heat treatment (1300 K, 6 h). The density of boundaries (surface per unit volume) with disorientation angles above 2° (S_V) is also provided. Furthermore, the mean disorientation angle ($\bar{\theta}$) is given. For calculation of the fractions of low-angle boundaries (x_{LAB}) and high-angle boundaries (x_{HAB}), threshold angles of 2° and 15° were chosen, respectively. The fraction of CSL boundaries (x_{CSL}) includes all CSL boundaries from $\Sigma 3$ to $\Sigma 25$ (Brandon's criterion, exponent was set to -0.5) which are also included in the fraction of high-angle boundaries. The standard deviation was calculated between values of the four EBSD scans for each of the samples respectively.

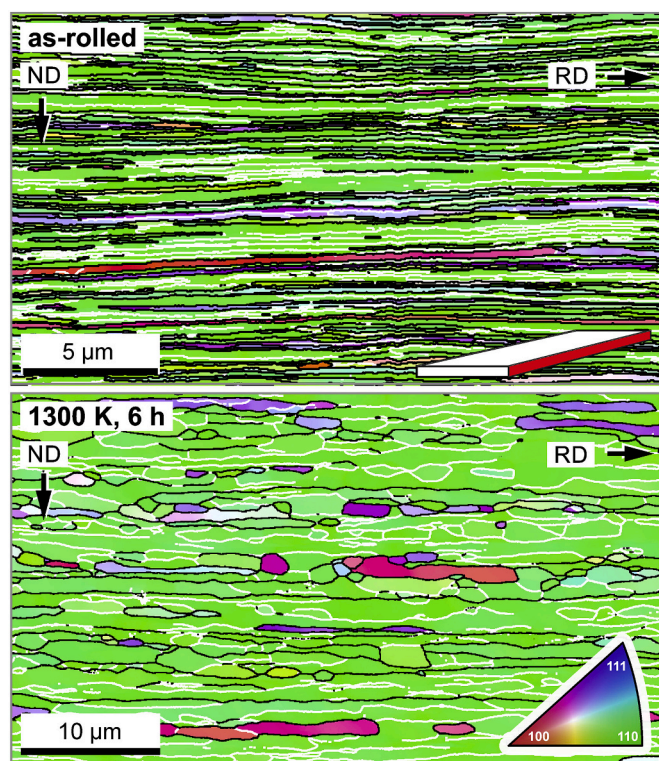


Fig. 6. Grain structure before and after annealing at 1300 K for 6 h. The orientation maps acquired by EBSD show the crystal direction along the RD according to the inverse pole figure (IPF) displayed in the lower inset. As a reference, the as-rolled state (top) is shown above the heat-treated microstructure (bottom). The top inset shows the examined surface (highlighted in red). Note the different magnifications of the maps. High-angle boundaries with a disorientation angle above a threshold value of 15° are highlighted in black, low-angle boundaries (2° – 15°) are represented by white lines. (For interpretation of the references to colour in this figure legend, the reader is referred to the web version of this article.)

chord lengths for HABs times the mean chord length for HABs ($\bar{\lambda}_{HAB}$) is displayed versus the chord lengths for HABs (λ_{HAB}) normalized by the mean chord length for HABs. At first glance, the distribution of the chord lengths for HABs seems quite similar to the above-mentioned distributions. The best fits of the data using a single lognormal distribution are displayed in Fig. 8 by solid lines of the same color as the respective data points. Unlike the chord lengths for all boundaries, the description of the chord lengths for HABs by a single lognormal distribution reveals a deviation between function graphs and experimental data for both material conditions. This mismatch is evident for chord lengths for HABs larger than the most probable fraction for both material conditions, but in a particularly clear manner after annealing. The probability density of chord lengths for HABs slightly larger than the chord length with maximal probability is overestimated by the function graphs drawn in the same color of the data points. For even larger chord

lengths, however, the probability density is underestimated. This indicates that the hypothesis about a lognormal distribution of chord lengths for HABs is not suitable, independent whether the material is in as-rolled or annealed condition. Studying Fig. 6 in this light again, the maps displaying the as-rolled material and the annealed condition exhibit some grains with remarkably larger chord lengths for HABs in comparison to the mean values. These grains possess in comparison to the smaller grains a distinct subgrain structure highlighted by the white boundaries.

The mismatch between the distributions of chord length for HABs and the respective single lognormal distributions might be originated in the following issues: (i) The selected distribution function is incorrect and/or (ii) the experimental data are non-unimodally distributed. Therefore, an attempt was made to describe the distributions of chord length for HABs by a superposition (solid red line) of two lognormal distributions (dashed red lines labeled as (1) and (2) in Fig. 8), whereby distribution (1) describes the chord length around the highest probability density and distribution (2) the distribution at larger chord lengths. The match of experimental data and solid red function graphs demonstrates that a superposition of two lognormal distributions is necessary and sufficient for a proper description of the distribution of chord length for HABs.

The origin of the bimodality in the distribution of chord lengths for HABs after rolling and its increase during annealing has not yet been clarified yet. However, we are convinced that this behavior is linked with the strong texture of the as-rolled W sheets and the further sharpening during subsequent annealing. As already has been discussed in connection with the sharpening of the texture, grains with orientations near the rotated cube component grow preferentially during annealing. Due to that, grains with other orientations are consumed gradually. Consequently, grains with orientations close to the rotated cube component, which were well-separated before the collapse of the lamellar microstructure, might develop into a single grain, having only a LAB at the connecting boundary, cf. Fig. 9 in the next section of this paper. This effect is known as grain coalescence and the replacement of the HAB by a remarkably less mobile LAB can be treated as kind of orientation pinning [61]. To investigate the validity of this hypothesis, the (dashed red) lognormal distributions in Fig. 8 were studied in more detail in the condition before and after annealing. By integrating the displayed graphs we derived the areas and fractions, related to the single distributions. A comparison of the fractions in the as-rolled and the annealed condition reveals a decrease of the fraction related to distribution (1) containing the grains belonging to the distribution describing the probability density of the chord lengths for HABs around the maximum. This fraction is reduced from 81% to 67% and proves the trend of the increase in fraction in favor of distribution (2), describing the distribution of larger chord length, at the expense of distribution (1). This increase in fraction of distribution (2) results in a stronger bimodality of the distribution of chord lengths for HABs, at least in this relatively early state of microstructural restoration.

Fig. 9a shows the surface density (S_V) for boundaries (starting with a disorientation angles of 2°) in dependence on the disorientation angle. A clear reduction from the as-rolled to the annealed condition is

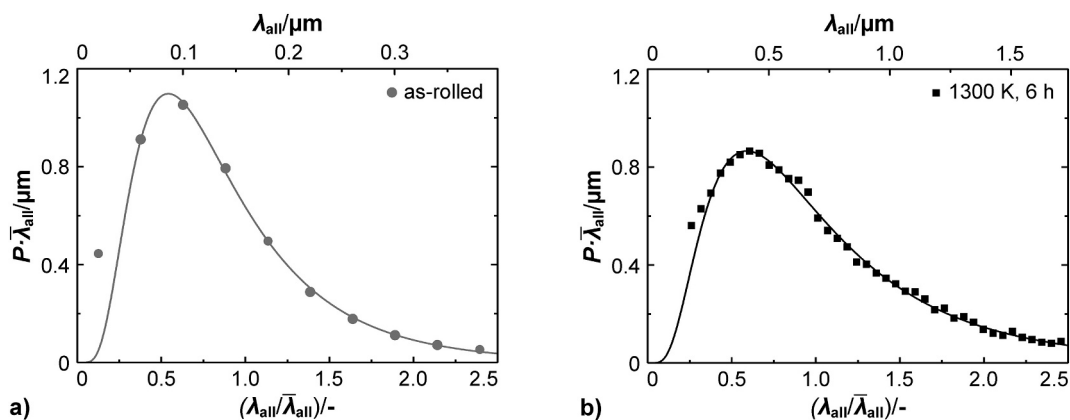


Fig. 7. Distribution of the chord lengths for all boundaries. Both diagrams display the probability density (P) multiplied with the mean chord length for all boundaries ($\bar{\lambda}_{all}$) that is plotted against the chord length for all boundaries (λ_{all}) normalized to the mean chord length for all boundaries. Subplot (a) shows the results for the as-rolled condition and (b) after annealing at 1300 K for 6 h. The experimental data were fitted using lognormal distributions.

observed. The boundary density of HABs is reduced by a much larger extent than the boundary density of LABs. Due to that, a decrease of the mean disorientation angle from $29.5 \pm 0.6^\circ$ to $19.4 \pm 1.3^\circ$ took place during annealing. Furthermore, the dominating type of boundary is reversed: in the as-rolled condition, 68% of all boundaries are HABs and 32% LABs, whereas in the annealed condition 43% of the boundaries are HABs and 57% LABs. This change in fractions seems to be a striking feature of the strongly textured material investigated in this study and has not been reported in previous studies on the microstructural evolution of rolled W during annealing, cf. e.g. Ref. [21, 22, 50, 62].

The preferred coarsening of grains with α -fiber orientation in strongly textured W sheets is assumed to have an impact on the dominating type of boundary, HAB or LAB. Due to the consumption of γ -fiber grains by the α -fiber grains during annealing, an increasing fraction of boundaries is located between different α -fiber grains only. This assumption is supported by the uncorrelated misorientation distributions displayed in Fig. 9b showing the probability density (P) of boundaries with certain disorientation angles (θ) after randomizing the coordinates of the pixels in the EBSD data file (used python script is provided as supplementary material). Due to the strong texture, the as-rolled W possesses a strong deviation from the so-called Mackenzie distribution describing the distribution of disorientations for randomly distributed orientations e.g. in a texture-free polycrystal [63]. In the

displayed distribution, the probability density of boundaries with a disorientation angle below 30° are more abundant than in the Mackenzie distribution. In contrast to that, the probability density of boundaries with a larger disorientation angle is clearly lower. After annealing, a hump has formed in the LAB regime around 10° and the probability densities at larger disorientation angles are further reduced while maintaining a peak around 55° . This indicates that a considerable fraction of LABs in the annealed condition is not to be considered as deformation-induced dislocation boundaries, rather than as former grain boundaries which have impinged on each other and formed LABs a consequence of the sharpening of the texture.

Changes in dislocation density by annealing were quantified by applying the modified Williamson-Hall method. After annealing at 1300 K for 6 h a dislocation density of $1.9 \cdot 10^{13} \text{ m}^{-2}$ was derived. In comparison to the result of the as-rolled condition [13], which was derived by the modified Williamson-Hall method as well, this is a decrease in dislocation density by around two orders of magnitude: from $8.8 \cdot 10^{14} \text{ m}^{-2}$ to $1.9 \cdot 10^{13} \text{ m}^{-2}$. Our result ($1.9 \cdot 10^{13} \text{ m}^{-2}$) is clearly below the dislocation density of $1.9 \cdot 10^{14} \text{ m}^{-2}$ given in a recent TEM study conducted by Ren et al. [62] after annealing of rolled W at 1473 K for 1 h, labeled as recovered. For fully recrystallized W, which has been annealed at 1873 K for 1 h, Oh et al. [64] have determined by the Williamson-Hall method a significantly lower dislocation density of

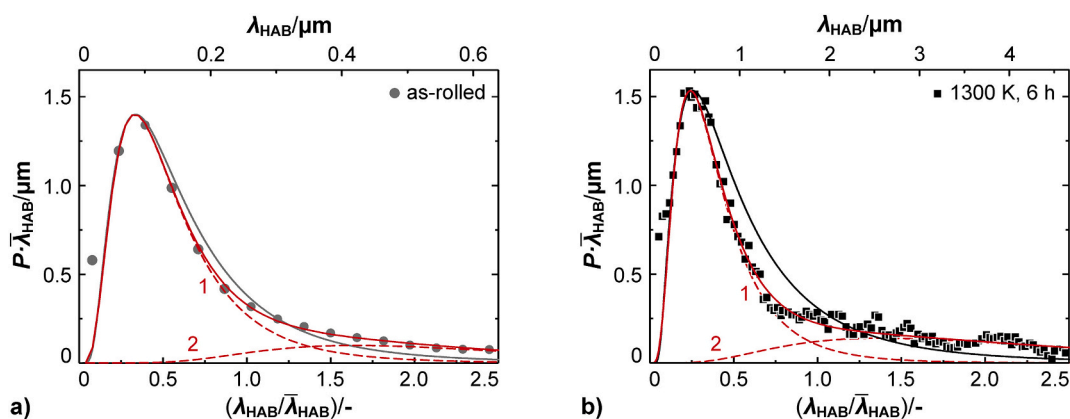


Fig. 8. Evolution of the distribution of the chord lengths for HABs. In both subplots, the probability density (P) multiplied with the mean chord length for all boundaries ($\bar{\lambda}_{all}$) is plotted against the chord length for all boundaries (λ_{all}) normalized to the mean chord length for all boundaries. Grey circles represent the as-rolled condition (a), whereas black squares display the chord length distributions of the annealed state (1300 K, 6 h), subplot (b). The fit lines are based on a lognormal distribution [60]. The grey and black function graphs showing the attempt to describe the experimental data using a single lognormal distribution. Furthermore, an attempt was made to describe the experimental distributions by a superposition of two lognormal distributions. The superpositions are shown as solid red lines, the single distributions labeled as (1) and (2) are represented by the dashed red lines. (For interpretation of the references to colour in this figure legend, the reader is referred to the web version of this article.)

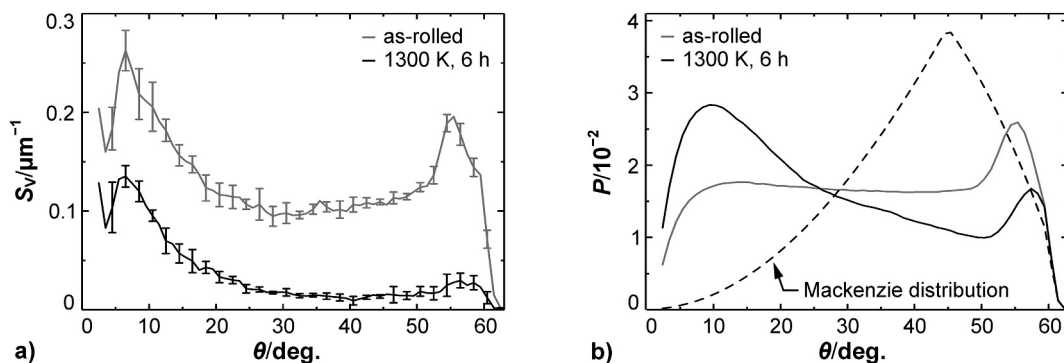


Fig. 9. Disorientation distributions. In (a) the boundary density (S_v) is plotted against the (correlated) disorientation angle (θ) for the as-rolled and annealed condition. The data are displayed using a bin width of 1° . Error bars (only shown in 2° steps for better readability) represent the standard deviation of the boundary density for a given disorientation angle calculated from the different areas scanned for each material. (b) Uncorrelated misorientation distribution functions. The disorientation distribution after a randomization of the pixel coordinates is shown. The grey distribution represents the probability density (P) as a function of the disorientation angle (θ) for the as-rolled condition. The black solid line displays the distribution after annealing. The black dashed line shows the theoretic Mackenzie distribution of a texture-free material with cubic crystal lattice. A bin width of 1° was chosen.

$1.6 \cdot 10^{12} \text{ m}^{-2}$. Since the annealed material in the present study is in between, not recrystallized but strongly recovered, our determined value of dislocation density has a plausible magnitude, located in a regime below the as-rolled condition and the short time annealing by Ren et al. [62] but above the value reported by Oh et al. [64].

Although the loss in hardness of severely cold-rolled W follows a logarithmic Kuhlmann relationship, localized short-range motion of HABs and the sharpening of the deformation texture during annealing clearly delineate the underlined softening process from classical dislocation-mediated recovery. Furthermore, the lack of distinct recrystallization fronts, that are separating deformed and newly created dislocation-free areas, and the continuous manner of microstructural modification during annealing precludes discontinuous recrystallization [65] as softening mechanism. Instead, all microstructural modifications discussed so far are pointing to extended recovery. Extended recovery is related to materials that have undergone large strains and formed a lamellar, HAB-rich microstructure during deformation, which starts to break-up and spheroidizes [58]. This prerequisite applies well to the as-rolled condition of the cold-rolled W studied in this work.

Furthermore, the HAB fraction of 68% indicates that the microstructure might have become resistant against discontinuous recrystallization. The sufficient fraction of HABs needed to suppress discontinuous recrystallization cannot fairly be quantified precisely but is assumed to be in the range between 60 and 70% [53]. With an annealing temperature of 1300 K, the coarsening of the microstructure described in this study took place significantly below the temperatures (around 1500 K) that are known to cause the onset of discontinuous recrystallization during short-time annealing in less deformed W [66]. Taking into account the large extent of microstructural modifications of severely rolled W during annealing, the remarkable drop in hardness in the early stage of annealing as displayed in Fig. 2 would be the logical consequence of extended recovery, which presumably has taken place. In our point of view, also the phenomenon of 45° embrittlement is closely linked with this kind of material softening by extended recovery.

3.4. The 45° embrittlement of rolled W sheets

In this section, we revisit the issue of 45° embrittlement considering the annealing-induced shift of BDT temperature, microstructural coarsening and rolling texture as discussed above. Here we show that the phenomenon of so-called 45° embrittlement needs to be comprehended as a combined effect of texture and the increased mean chord length for all boundaries after annealing.

In order to gain a better assessment of the impact of 45° fracture on the brittle material behavior after annealing at 1300 K for 6 h, we made an attempt to correlate the increased BDT temperature with the evolution of the microstructure. Between BDT temperature and grain size, an empirical relation following a Hall–Petch-like relationship was proven in many studies, e. g. Ref. [8, 10, 67]. Recently, we have shown that the application of this relation using the mean chord length for HABs is also well suited describing the different BDT temperatures of W sheets warm-rolled to various levels of deformation [10]. For the regime of mean chord length this study is dealing with, Reiser et al. [68] have suggested that the mean distance between assisted dislocation nucleation along the crack front is the relevant parameter controlling the BDT temperature. Fig. 10 shows the BDT temperatures of W sheets differing in production history displayed versus the mean chord length for HABs (a) and the mean chord length for all boundaries (b). Additionally to the W sheet annealed at 1300 K for 6 h represented by a red square, also experimental data from an earlier study on warm- and cold-rolled W sheets in as-rolled condition [10] are displayed (warm-rolled W is highlighted by open circles and the cold-rolled sheet by a black circle). To get an idea of the material behavior of undeformed W, we also consider the data of a fully recrystallized W sheet (open square), which was warm-rolled to a logarithmic thickness reduction of 1.7 before annealing in a hydrogen furnace at 2300 K for a duration of 1 h. All BDT temperatures shown here have been determined under the use of an identical experimental setup [10]. At first glance, a comparison of data points and a linear regression line in Figs. 10a and 10b reveals a good match. In the given set of materials, both microstructural parameters are suited to derive expectable BDT temperatures for these materials. On second view, however, the attempt to correlate BDT temperature with the mean chord length for all boundaries appears more promising.

From the correlation Fig. 10b is revealing, a general behavior can be derived concerning the BDT temperature of polycrystalline W sheets. In the studied parameter range (cf. Table 3), the BDT temperature of materials in as-rolled condition and annealed ones follows a Hall–Petch-like relationship between BDT temperature and the mean chord length for all boundaries causing a reduction in BDT temperature with decreasing mean chord length. Applying this relationship reveals that under the given experimental boundary conditions W becomes ductile at room temperature ductile if the mean spacing between all boundaries is about or below $0.2 \mu\text{m}$. As a result of microstructural coarsening, the excellent ductility of the as-rolled condition at room temperature is lost after annealing. Figure 10 also shows that the W sheet showing 45° embrittlement (1300 K, 6 h) follows the trend of increasing BDT

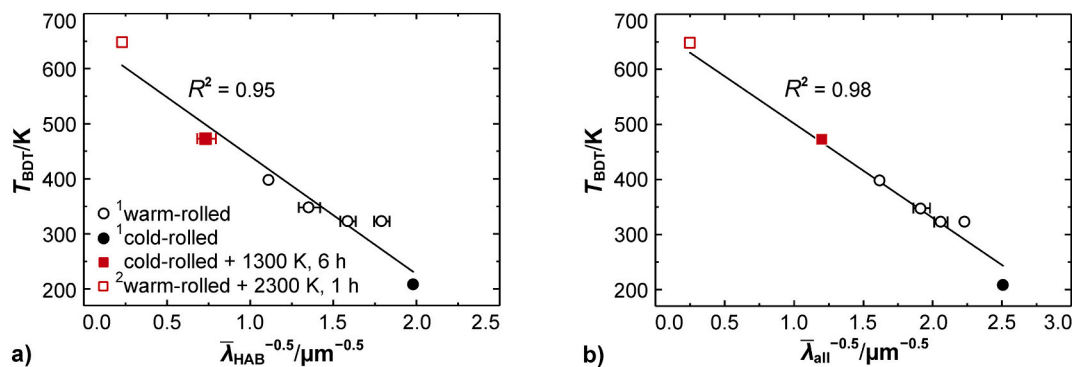


Fig. 10. Correlation between BDT temperature and chord length. In (a) the BDT temperature (T_{BDT}) is plotted against the mean chord length for HABs ($\bar{\lambda}_{HAB}$) given as one divided by the square root of the mean chord length for HABs. In subplot (b) BDT temperature is plotted against mean chord length for all boundaries ($\bar{\lambda}_{all}$) in the same manner. The BDT temperatures of the warm-rolled materials and the cold-rolled sheet are displayed by open and full circles, respectively. The data of the as-rolled conditions (superscripted 1) have been published in Ref. [10]. Please note slight differences in BDT temperature compared to Ref. [10] due to the application of different criteria for the BDT temperature. The red filled square represents the BDT temperature of the annealed sample of the current study. Furthermore, the BDT temperature of fully recrystallized W (superscripted 2) is given by a red open square [25]. (For interpretation of the references to colour in this figure legend, the reader is referred to the web version of this article.)

temperature with a growing mean chord length for all boundaries. The match of the regression line and the BDT temperatures of this material supports the conclusion drawn above, that 45° fracture is an intrinsic feature of W sheets with strong bcc rolling texture and does not signal embrittlement of the material in terms of an increased BDT temperature. The increased mean chord length for all boundaries after annealing (1300 K, 6 h) seems to be solely responsible for the determined shift in BDT temperature from 208 K to 473 K.

Considering that even in strongly textured W sheets in the as-rolled condition cleavage fracture takes place with 45° to the rolling direction (cf. Fig. 4) as well as the found Hall–Petch-like relationship, in our opinion the following conclusion becomes evident: the phenomenon of so-called 45° embrittlement needs to be comprehended as a consequence of two separated effects, causing clearly distinguishable consequences: (i) The strong rotated cube component in rolled W sheets, which further increases in intensity during annealing, in combination with the {001} plane as the favorable cleavage plane in W [56,57], is the origin for the preferred crack path aligned 45° to the rolling direction. (ii) Losing room-temperature ductility by presumably extended recovery during annealing, however, is a result of the microstructural coarsening. We identified the mean chord length for all boundaries as a critical microstructural parameter. Due to the increase of the latter during annealing, cold-rolled W suffers a loss of the advantages gained by the cold working process and the material exhibits brittle material behavior at room temperature anew. Consequently, with this work, we demonstrate the need for a stabilized microstructure before the utilization of cold-rolled W in high-temperature applications can be achieved successfully.

Table 3

Summary of data displayed in Fig. 10. For all displayed materials the mean chord length for HABs ($\bar{\lambda}_{HAB}$) and mean chord length for all boundaries ($\bar{\lambda}_{all}$) are listed. Furthermore, the resulting BDT temperatures (T_{BDT}) and the applied loading rates (dK/dt) are given. Warm-rolled materials are denoted as WR, cold rolling is indicated by CR after the value of logarithmic strain conducted by rolling. The data of the as-rolled conditions and the recrystallized material have been published in Ref. [10, 25]. Please note the slight differences in BDT temperature and chord length in comparison to Ref. [10] due to the use of different criteria for the definition of the BDT temperature and new EBSD measurements on the same materials possessing a much better statistics.

Material	T_{BDT}/K	$dK/dt/MPa\ m^{0.5}\ s^{-1}$	$\bar{\lambda}_{HAB}/\mu m$	$\bar{\lambda}_{all}/\mu m$
1.7WR, as-rolled	398	1.00 ± 0.06	0.811 ± 0.021	0.382 ± 0.016
2.5WR, as-rolled	348	1.08 ± 0.04	0.547 ± 0.051	0.272 ± 0.017
2.9WR, as-rolled	323	1.03 ± 0.06	0.397 ± 0.023	0.236 ± 0.011
3.3WR, as-rolled	323	1.18 ± 0.05	0.312 ± 0.016	0.201 ± 0.004
4.1CR, as-rolled	208	1.08 ± 0.11	0.255 ± 0.005	0.159 ± 0.002
4.1CR, 1300 K, 6 h	473	1.04 ± 0.20	1.866 ± 0.280	0.694 ± 0.022
1.7WR, 2300 K, 1 h	648	3.90 ± 0.06	21.26 ± 0.34	17.72 ± 0.33

4. Conclusions

The fine-grained and dislocation-rich microstructure of technically pure, room-temperature ductile W sheets raises questions about the thermal stability of this material. In this work, we conducted isothermal heat treatments at 1300 K in the range between 0.1 h and 210 h combined with subsequent mechanical and microstructural studies on an undoped W sheet that has undergone severely rolling deformation. Referring to the main questions outlined in the introduction section, our findings can be summarized as follows:

(1.1) The BDT temperature increases from 208 K to 473 K already after 6 h of annealing at 1300 K. This annealing procedure transforms the sharp BDT into a wide transition regime, spanning over more than 200 K.

(1.2) Loss in hardness of severely cold-rolled W follows a logarithmic Kuhlmann relationship in the investigated time range. An apparent activation volume of the responsible restoration process of $28b^3$ confirms the trend towards lower apparent activation volumes with increasing level of deformation.

(1.3) Coarsening of the lamellar microstructure is evident already after an annealing duration of 6 h at 1300 K. Coarsening in this early stage of annealing, its gradual manner, and the fact that grain coarsening takes place at a relatively low annealing temperature are pointing to extended recovery as responsible restoration process in severely deformed cold-rolled W sheets.

(2.1) The phenomenon of 45° embrittlement needs to be comprehended as a combined effect of rolling texture and increased BDT temperature after annealing. Below the BDT temperature, crack growth in W sheets with a strong rotated cube texture component propagates

always with an inclination angle of 45° to the rolling direction, whether in the as-rolled or the annealed condition.

(2.2) The BDT temperature correlates with the mean chord length for all boundaries following a Hall–Petch-like relationship. Coarsening of the microstructure during annealing causes consequently brittle material behavior at room temperature.

In summary, the most important finding of this work is the revealing of the loss of room-temperature ductility in conjunction with the appearance of 45° embrittlement as a consequence of the rapid collapse of the lamellar microstructure of the as rolled condition, that takes place at a relatively low annealing temperature. This shows that before room-temperature ductile, cold-rolled W will be suitable for utilization in high-temperature applications, the fine-grained microstructure has to be stabilized. Care must be taken if technically pure, cold-rolled W sheets are used in laminate production, are brazed during the preparation process for any tests or are tested under the exposure of heat. Furthermore, our experiments provide strong evidence that for an effective prevention of 45° embrittlement microstructural modifications during processing need to be given greater attention. The correlations prove that the rapid coarsening of the as-rolled microstructure in cold-rolled W sheets is raising the BDT temperature clearly above room

temperature causing in combination with the very high orientation density of the rotated cube component brittle material behavior showing 45° fracture.

Declaration of competing interest

The authors declare that they have no conflict of interests.

Acknowledgments

We gratefully acknowledge our gratitude to Hannes Traxler, Plansee SE, for providing recrystallized W specimens. Furthermore, we like to thank Siegfried Baumgärtner, KIT, for his support concerning the fracture toughness tests. This work has been carried out within the framework of the EUROfusion Consortium and has received funding from the Euratom research and training program 2014-2018 and 2019-2020 under grant agreement No 633053. The views and opinions expressed herein do not necessarily reflect those of the European Commission.

Appendix

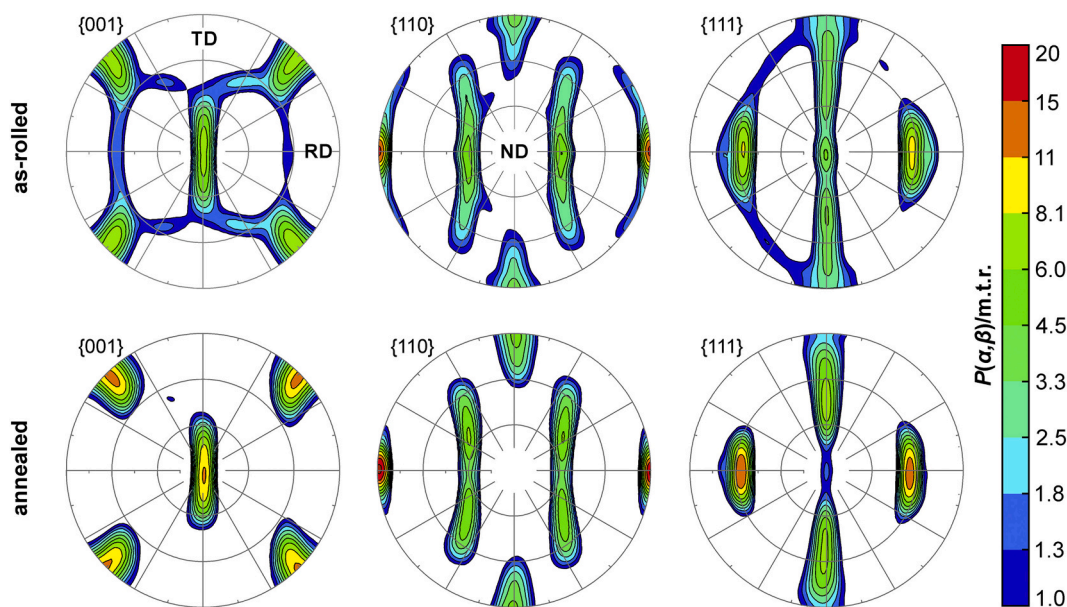


Fig. A1. Calculated pole figures of the as-rolled condition and after annealing at 1300 K for 6 h from EBSD orientation measurements. The pole densities (P) are given as multiple times random (m.t.r.) of a material with cubic crystal lattice having no texture.

Appendix A. Supplementary data

Supplementary data to this article can be found online at <https://doi.org/10.1016/j.ijrmhm.2020.105347>.

References

- [1] B. Šesták, A. Seeger, *Gleitung und Verfestigung in kubisch-raumzentrierten Metallen und Legierungen* (I), *Z. Metallkunde* 69 (4) (1978) 195–202.
- [2] L. Hollang, *Mechanical properties*, in: Y. Waseda, M. Isshiki (Eds.), *Purification Process and Characterization of Ultra High Purity Metals*, Springer, Berlin, DEU, 2002, pp. 305–348.
- [3] I. Smid, M. Akiba, G. Vieider, et al., Development of tungsten armor and bonding to copper for plasma-interactive components, *J. Nucl. Mater.* 258–263 (1998) 160–172, [https://doi.org/10.1016/S0022-3115\(98\)00358-4](https://doi.org/10.1016/S0022-3115(98)00358-4).
- [4] S. Nogami, S. Watanabe, J. Reiser, et al., A review of impact properties of tungsten materials, *Fusion Eng. Des* 135 (2018) 196–203, <https://doi.org/10.1016/j.fusengdes.2018.08.001>.
- [5] J.P. Morniroli, *Low-temperature embrittlement of undoped and doped tungsten*, in: E. Pink, L. Bartha (Eds.), *The Metallurgy of Doped/Non-sag Tungsten*, Elsevier, London, GBR, 1989, pp. 235–250.
- [6] Q. Wei, L.J. Kecskes, Effect of low-temperature rolling on the tensile behavior of commercially pure tungsten, *Mater. Sci. Eng. A* 491 (1–2) (2008) 62–69, <https://doi.org/10.1016/j.msea.2008.01.013>.
- [7] A.A.N. Németh, J. Reiser, D.E.J. Armstrong, et al., The nature of the brittle-to-ductile transition of ultra fine grained tungsten (W) foil, *Int. J. Refract. Met. Hard Mater.* 50 (2015) 9–15, <https://doi.org/10.1016/j.ijrmhm.2014.11.005>.
- [8] J. Reiser, J. Hoffmann, U. Jäntschi, et al., Ductilisation of tungsten (W), *Int. J. Refract. Met. Hard Mater.* 54 (2016) 351–369, <https://doi.org/10.1016/j.ijrmhm.2015.09.001>.
- [9] V. Nikolić, S. Wurster, D. Firmeis, et al., Improved fracture behavior and microstructural characterization of thin tungsten foils, *Nucl. Mater. Energy* 9 (2016)

- 181–188, <https://doi.org/10.1016/j.nme.2016.06.003>.
- [10] C. Bonnekoh, A. Hoffmann, J. Reiser, The brittle-to-ductile transition in cold rolled tungsten, *Int. J. Refract. Met. Hard Mater.* 71 (71) (2018) 181–189, <https://doi.org/10.1016/j.ijrmhm.2017.11.017>.
- [11] V. Nikolić, S. Wurster, D. Firneis, et al., Fracture toughness evaluation of UFG tungsten foil, *Int. J. Refract. Met. Hard Mater.* 76 (2018) 214–225, <https://doi.org/10.1016/j.ijrmhm.2018.06.008>.
- [12] J. Reiser, M. Rieth, B. Daffermer, et al., Charpy impact properties of pure tungsten plate material in as-received and recrystallized condition, *J. Nucl. Mater.* 442 (1–3) (2013) S204–S207, <https://doi.org/10.1016/j.jnucmat.2012.10.037>.
- [13] C. Bonnekoh, U. Jäntschi, J. Hoffmann, et al., The brittle-to-ductile transition in cold rolled tungsten plates, *Int. J. Refract. Met. Hard Mater.* 78 (78) (2019) 146–163, <https://doi.org/10.1016/j.ijrmhm.2018.09.010>.
- [14] N. Hansen, C.Y. Barlow, Plastic deformation of metals and alloys, in: D.E. Laughlin, K. Hōno (Eds.), *Physical Metallurgy*, 5th ed., Elsevier, Amsterdam, NLD, 2014, pp. 1681–1764, <https://doi.org/10.1016/B978-0-444-53770-6.00017-4>.
- [15] X.-X. Zhang, Q.-Z. Yan, C.-T. Yang, et al., Recrystallization temperature of tungsten with different deformation degrees, *Rare Metals* 35 (7) (2016) 566–570, <https://doi.org/10.1007/s12598-014-0315-2>.
- [16] J.L. Ratliff, H.R. Ogden, A compilation of the tensile properties of tungsten, DMIC Memorandum 157. Battelle Memorial Institute, 1962Columbus, OH, USA.
- [17] U.M. Ciucani, A. Thum, C. Devos, et al., Recovery and recrystallization kinetics of differently rolled, thin tungsten plates in the temperature range from 1325 °C to 1400 °C, *Nucl. Mater. Energy* 20 (2019) 100701, <https://doi.org/10.1016/j.nme.2019.100701>.
- [18] K. Farrell, A.C. Schaffhauser, J.O. Stiegler, Recrystallization, grain growth and the ductile-brittle transition in tungsten sheet, *J. Less Common Metals* 13 (2) (1967) 141–155, [https://doi.org/10.1016/0022-5088\(67\)90177-4](https://doi.org/10.1016/0022-5088(67)90177-4).
- [19] J. Webb, S. Gollapudi, I. Charit, An overview of creep in tungsten and its alloys, *Int. J. Refract. Met. Hard Mater.* 82 (2019) 69–80, <https://doi.org/10.1016/j.ijrmhm.2019.03.022>.
- [20] J.L. Ratliff, D.J. Maykuth, H.R. Ogden, et al., Development of a Ductile Tungsten Sheet Alloy, Research Report AD 277459, Bureau of Naval Weapons, Battelle Memorial Institute, Columbus, OH, USA, 1962.
- [21] A. Alfonso, D. Juul Jensen, G.-N. Luo, et al., Recrystallization kinetics of warm-rolled tungsten in the temperature range 1150–1350°C, *J. Nucl. Mater.* 455 (1–3) (2014) 591–594, <https://doi.org/10.1016/j.jnucmat.2014.08.037>.
- [22] A. Alfonso, D. Juul Jensen, G.-N. Luo, et al., Thermal stability of a highly-deformed warm-rolled tungsten plate in the temperature range 1100–1250°C, *Fusion Eng. Des.* (2015) 98–99, <https://doi.org/10.1016/j.fusengdes.2015.05.043> 1924–1928.
- [23] J. Neges, B. Ortner, G. Leichtfried, et al., On the 45° embrittlement of tungsten sheets, *Mater. Sci. Eng. A* 196 (1–2) (1995) 129–133, [https://doi.org/10.1016/0921-5093\(94\)09706-2](https://doi.org/10.1016/0921-5093(94)09706-2).
- [24] V.I. Trefilov, Y.V. Milman, Physical basis of thermomechanical treatment of refractory metals, in: H. Bildstein, H.M. Ortner (Eds.), *12th International Plansee Seminar '89: Proceedings, Metallwerk Plansee, Reutte, AUT, 1989*, pp. 107–131.
- [25] C. Bonnekoh, J. Reiser, A. Hartmaier, et al., The brittle-to-ductile transition in cold-rolled tungsten sheets: the rate-limiting mechanism of plasticity controlling the BDT in ultrafine-grained tungsten, *J. Mater. Sci.* 55 (26) (2020) 12314–12337, <https://doi.org/10.1007/s10853-020-04801-5>.
- [26] ASTM International, *Electrolytic Polishing of Metallographic Specimens*, 9th ed. (E1558), ASTM International, West Conshohocken, PA, USA, 2014.
- [27] Deutsche Institut für Normung e.V. DIN, *Metallic Materials – Vickers hardness Test. (6507-1)*, Beuth, Berlin, DEU, 2005.
- [28] ASTM International, *Linear-Elastic Plane-Strain Fracture Toughness K1C of Metallic Materials*, 12th ed.(E399), ASTM International, West Conshohocken, PA, USA, 2012.
- [29] T.L. Anderson, *Fracture Mechanics*, CRC Press, Boca Raton, FL, USA, 2017, <https://doi.org/10.1201/9781315370293>.
- [30] P. Jepson, R. Bailey, A new method for quantification of texture uniformity of plate, in: A.D. Rollett (Ed.), *Applications of Texture Analysis*, John Wiley & Sons, Hoboken, NJ, USA, 2008, pp. 135–145.
- [31] S.I. Wright, M.M. Nowell, J.F. Bingert, A comparison of textures measured using X-ray and electron backscatter diffraction, *Metall. Mater. Trans. A* 38 (8) (2007) 1845–1855, <https://doi.org/10.1007/s11661-007-9226-2>.
- [32] K. Davut, S. Zaefferer, Improving the reliability of EBSD-based texture analysis by a new large area mapping technique, in: A. Tewari (Ed.), *Textures of Materials - ICOTOM 16*, Trans. Tech. Publ., Dürnten-Zürich, CHE, 2012, pp. 566–569, <https://doi.org/10.4028/www.scientific.net/MSF.702-703.566>.
- [33] U.F. Kocks, Kinematics and kinetics of plasticity, in: U.F. Kocks, C.N. Tomé, H.-R. Wenk (Eds.), *Texture and Anisotropy*, 1st ed., Cambridge Univ. Press, Cambridge, GBR, 2000, pp. 326–389.
- [34] H.-J. Bunge, *Texture Analysis in Materials Science*, Butterworth & Co, Burlington, MA, USA, 1982, <https://doi.org/10.1016/C2013-0-11769-2>.
- [35] N. Bozzolo, F. Gerspach, G. Sawina, et al., Accuracy of orientation distribution function determination based on EBSD data-A case study of a recrystallized low alloyed Zr sheet, *J. Microsc.* 227 (3) (2007) 275–283, <https://doi.org/10.1111/j.1365-2818.2007.01811.x>.
- [36] B. Fultz, J.M. Howe, *Transmission Electron Microscopy and Diffraction of Materials*, Springer, Berlin, DEU, 2008, <https://doi.org/10.1007/978-3-540-73886-2>.
- [37] B.D. Cullity, S.R. Stock, *Elements of X-ray Diffraction*, Pearson Education, Harlow, GBR, 2014.
- [38] T. Ungár, Strain broadening caused by dislocations, in: R. Delhez, E.J. Mittemeijer (Eds.), *Proceedings of the Fifth European Powder Diffraction Conference*, Trans. Tech. Publ., Uetikon-Zürich, CHE, 1998, pp. 151–157, <https://doi.org/10.4028/www.scientific.net/MSF.278-281.151>.
- [39] G. Ribárik, T. Ungár, Characterization of the microstructure in random and textured polycrystals and single crystals by diffraction line profile analysis, *Mater. Sci. Eng. A* 528 (1) (2010) 112–121, <https://doi.org/10.1016/j.msea.2010.08.059>.
- [40] U.M. Ciucani, A. Thum, C. Devos, et al., Isothermal annealing of thin rolled tungsten plates in the temperature range from 1300 °C to 1400 °C, *Nucl. Mater. Energy* 15 (2018) 128–134, <https://doi.org/10.1016/j.nme.2018.03.009>.
- [41] V. Nikolić, J. Riesch, R. Pippan, The effect of heat treatments on pure and potassium doped drawn tungsten wires: Part I, *Mater. Sci. Eng. A* 737 (2018) 422–433, <https://doi.org/10.1016/j.msea.2018.09.027>.
- [42] S. Bonk, J. Reiser, J. Hoffmann, et al., Cold rolled tungsten (W) plates and foils, *Int. J. Refract. Met. Hard Mater.* 60 (2016) 92–98, <https://doi.org/10.1016/j.ijrmhm.2016.06.020>.
- [43] P. Lied, C. Bonnekoh, W. Pantleon, et al., Comparison of K-doped and pure cold-rolled tungsten sheets: as-rolled condition and recrystallization behaviour after isochronal annealing at different temperatures, *Int. J. Refract. Met. Hard Mater.* 85 (2019) 105047, <https://doi.org/10.1016/j.ijrmhm.2019.105047>.
- [44] G.F. Vander Voort, R. Fowler, Low-load vickers microindentation hardness testing, *Adv. Mater. Process.* 170 (4) (2012).
- [45] D. Kuhlmann, Zur Theorie der Nachwirkungerscheinungen, *Z. Phys.* 124 (7–12) (1948) 468–481, <https://doi.org/10.1007/BF01668885>.
- [46] D. Kuhlmann, G. Masing, J. Raffelsieper, Zur Theorie der Erholung, *Z. Metallkde* 40 (7) (1949) 241–246.
- [47] E. Nes, Recovery revisited, *Acta Metall. Mater.* 43 (6) (1995) 2189–2207, [https://doi.org/10.1016/0956-7151\(94\)00409-9](https://doi.org/10.1016/0956-7151(94)00409-9).
- [48] H.P. Stüwe, A.F. Padilha, F. Siciliano, Competition between recovery and recrystallization, *Mater. Sci. Eng. A* 333 (1–2) (2002) 361–367, [https://doi.org/10.1016/S0921-5093\(01\)01860-3](https://doi.org/10.1016/S0921-5093(01)01860-3).
- [49] D. Tabor, *The Hardness of Metals*, Oxford Univ. Press, Oxford, GBR, 1951.
- [50] J. Reiser, C. Bonnekoh, T. Karcher, et al., Recrystallisation towards a single texture component in heavily cold rolled tungsten (W) sheets and its impact on micro-mechanics, *Int. J. Refract. Met. Hard Mater.* 86 (2020) 105084, <https://doi.org/10.1016/j.ijrmhm.2019.105084>.
- [51] A. Alfonso, *Thermal Stability of Warm-Rolled Tungsten*, Ph.D. Thesis Technical University of Denmark, Lyngby, DNK, 2015.
- [52] D. Caillard, J.-L. Martin, *Thermally Activated Mechanisms in Crystal Plasticity*, Pergamon, Oxford, GBR, 2003.
- [53] J. Humphreys, G.S. Rohrer, A.D. Rollett, *Recrystallization and Related Annealing Phenomena*, Elsevier, Amsterdam, NLD, 2017, <https://doi.org/10.1016/B978-0-08-044164-1.X5000-2>.
- [54] D. Raabe, Recovery and recrystallization: phenomena, physics, models, simulation, in: D.E. Laughlin, K. Hōno (Eds.), *Physical Metallurgy*, 5th ed., Elsevier, Amsterdam, NLD, 2014, pp. 2291–2397, <https://doi.org/10.1016/B978-0-444-53770-6.00023-X>.
- [55] B. Gludovatz, S. Wurster, A. Hoffmann, et al., A study into the crack propagation resistance of pure tungsten, *Eng. Fract. Mech.* 100 (2013) 76–85, <https://doi.org/10.1016/j.engfracmech.2012.07.021>.
- [56] J. Riedle, P. Gumbsch, H.F. Fischmeister, et al., Fracture studies of tungsten single crystals, *Mater. Lett.* 20 (5–6) (1994) 311–317, [https://doi.org/10.1016/0167-577X\(94\)90036-1](https://doi.org/10.1016/0167-577X(94)90036-1).
- [57] D. Hull, P. Beardmore, A.P. Valintine, Crack propagation in single crystals of tungsten, *Philos. Mag.* 12 (119) (1965) 1021–1041, <https://doi.org/10.1080/14786436508228132>.
- [58] P.B. Prangnell, J.S. Hayes, J.R. Bowen, et al., Continuous recrystallisation of lamellar deformation structures produced by severe deformation, *Acta Mater.* 52 (11) (2004) 3193–3206, <https://doi.org/10.1016/j.actamat.2004.03.019>.
- [59] J.-T. Park, J.A. Szpunar, Evolution of recrystallization texture in nonoriented electrical steels, *Acta Mater.* 51 (11) (2003) 3037–3051, [https://doi.org/10.1016/S1359-6454\(03\)00115-0](https://doi.org/10.1016/S1359-6454(03)00115-0).
- [60] G. Gottstein, *Physical Foundations of Materials Science*, Springer, Berlin, DEU, 2004, <https://doi.org/10.1007/978-3-662-09291-0>.
- [61] D.A. Hughes, N. Hansen, High angle boundaries formed by grain subdivision mechanisms, *Acta Mater.* 45 (9) (1997) 3871–3886, [https://doi.org/10.1016/S1359-6454\(97\)00027-X](https://doi.org/10.1016/S1359-6454(97)00027-X).
- [62] C. Ren, Z.Z. Fang, L. Xu, et al., An investigation of the microstructure and ductility of annealed cold-rolled tungsten, *Acta Mater.* 162 (2019) 202–213, <https://doi.org/10.1016/j.actamat.2018.10.002>.
- [63] A. Morawiec, Misorientation-angle distribution of randomly oriented symmetric objects, *J. Appl. Crystallogr.* 28 (3) (1995) 289–293, <https://doi.org/10.1107/S0021889894011088>.
- [64] Y. Oh, N. Kwak, K. Lee, et al., Ductility enhancement of tungsten after plastic deformation, *J. Alloys Compd.* 787 (2019) 801–814, <https://doi.org/10.1016/j.jallcom.2019.02.097>.
- [65] R.D. Doherty, D.A. Hughes, F.J. Humphreys, et al., Current issues in recrystallization: a review, *Mater. Sci. Eng. A* 238 (2) (1997) 219–274, [https://doi.org/10.1016/S0921-5093\(97\)00424-3](https://doi.org/10.1016/S0921-5093(97)00424-3).
- [66] E. Lassner, W.-D. Schubert, *Tungsten*, Kluwer Academic/Plenum Publishers, New York, NY, USA, 1999, <https://doi.org/10.1007/978-1-4615-4907-9>.
- [67] S. Nogami, A. Hasegawa, M. Fukuda, et al., Tungsten modified by potassium doping and rhenium addition for fusion reactor applications, *Fusion Eng. Des.* 152 (2020) 111445, <https://doi.org/10.1016/j.fusengdes.2019.111445>.
- [68] J. Reiser, A. Hartmaier, Elucidating the dual role of grain boundaries as dislocation sources and obstacles and its impact on toughness and brittle-to-ductile transition, *Sci. Rep.* 10 (1) (2020) 2739, <https://doi.org/10.1038/s41598-020-59405-5>.